Hindawi
Wireless Communications and Mobile Computing
Volume 2022, Article ID 5631787, 9 pages
https://doi.org/10.1155/2022/5631787

Research Article

Prediction of Air Leakage Rate of Sintering Furnace Based on BP Neural Network Optimized by PSO

Xiaokai Quan,[1] Nannan Zhang,[2] Guo Yu,[3] Qunfeng Liu,[4] and Lianbo Ma[1]

[1]*Department of Software Engineering, Northeastern University, Shenyang 110000, China*
[2]*Department of Physical Education, Northeastern University, Shenyang 110000, China*
[3]*Key Laboratory of Smart Manufacturing in Energy Chemical Process, Ministry of Education, East China University of Science and Technology, Shanghai 200000, China*
[4]*School of Computer Science and Technology, Dongguan University of Technology, Guangdong 523000, China*

Correspondence should be addressed to Guo Yu; guoyu@ecust.edu.cn

Received 14 March 2022; Revised 1 April 2022; Accepted 13 April 2022; Published 29 April 2022

Academic Editor: Xingsi Xue

Aiming at the difficulty of air leakage detection in the sintering process of the sintering furnace, especially the problems of high detection cost and poor timeliness of detection results when traditional methods are used for detection, we propose an air leakage rate prediction algorithm. Firstly, we use the particle swarm optimization algorithm to optimize the initial parameters of the neural network based on back propagation and get the best set of initial parameters through continuous search. Secondly, the optimized parameters are substituted into the neural network to train them with training data, and the trained parameters are obtained. Finally, the air leakage rate of the test set data is predicted by using the trained parameters. Compared with traditional calculation methods such as gas analysis and calorimetry, the proposed method can greatly simplify the detection process, shorten the detection time, and control the error within 5%, allowing the user to deal with the air leakage problem more timely and improve the overall sintering quality.

1. Introduction

With the development of the iron and steel industries, the demand for iron ore is increasing day by day. However, there is less and less rich ore that can be smelted directly into the furnace, so a large number of poor ore resources must be mined and used [1–4]. Direct smelting of lean ore into the furnace will worsen the production index of the blast furnace and reduce the economic benefit. Therefore, lean ore needs to be treated by beneficiation to select concentrate with high iron content, and fine ore produced in the mining and processing of concentrate and rich ore can only be used for blast furnace ironmaking after being lumped.

Iron ore powder agglomeration methods currently mainly include sintering and pelletizing. The production of pellets requires fine-grained concentrates and requires gas or liquid fuel for roasting. It has strong adaptability and can not only produce sintered ore with coarse-grained rich ore powder and concentrate, but also process industrial iron-containing wastes. Due to the dominance of the production of iron ore powder agglomeration, sintered ore accounts for 70% to 90% of the total iron-containing raw materials entering the furnace [5–8]. Therefore, sinter has always been the main raw material for blast furnace ironmaking. It mainly determines the technical and economic indicators of blast furnace smelting production [9–13]. In blast furnace ironmaking, the use ratio of sinter basically accounts for about 75% of the blast furnace burden and more than 70% of the blast furnace ironmaking cost and energy consumption. Therefore, the technical and economic indicators and quality of sintering production play a decisive role in the cost and effect of the blast furnace.

It can be seen that in the modern steel production process, sintering plays an irreplaceable role as an important link in providing raw materials for ironmaking blast furnaces in modern iron and steel production [14–20]. Using the sintering method to produce sinter not only solves the problem of fine ore ironmaking but also improves the

metallurgical properties of iron-containing raw materials, so that the production index and economic benefits of the blast furnace are obviously improved [21–25]. At present, the most commonly used sintering equipment in sintering production at home and abroad is the belt sintering machine, which provides most of the high-quality man-made rich ore required for the production of ironmaking blast furnaces. From the perspective of energy saving and environmental protection, the biggest disadvantage of the sintering machine is that its air leakage rate is high, resulting in diffuse noise in the vast space around the equipment.

During the sintering process, the negative pressure of the system will inevitably lead to a certain degree of air leakage between the material surface gap and the sidewall of the trolley, so that the air enters the sintering system from the position with poor sealing performance of the equipment, and at the same time reduces the working negative pressure of the sintering system [26–30].

The main causes of air leakage in sintering machines are (1) the gaps between trolleys and trolleys, between baffles and baffles, and between trolley grate bars and baffle pins; (2) the air leakage of the air duct and compensator of the small bellows is due to the rapid wear due to high temperature, air pumping, material scouring, and other reasons; (3) the sintering machine bellows head and tail. Under the action of high negative pressure in the large flue, a large amount of air is pumped into the head and tail spring sealing cover plates and the slideways on both sides; (4) wear air leakage of each connecting flange, pipeline, and bellows of the main exhaust system. More details of the air leakage of the sintering machine are referred to in [31].

The effective air volume per unit area of the sintering trolley reduces the output of the sintering machine and the quality of the sintered ore. The lower the unit effective air volume of the sintering system, the less sintered ore output there will be. In the sintering process, the electricity consumed by the fan accounts for more than 70% of the total electricity. If the air leakage rate is too high, the effective power of the fan will be greatly reduced. A large amount of air leakage not only affects the electricity consumption, but also affects the effective utilization of energy in the sintering process, and reduces the production efficiency, finally increasing the energy consumption in sintering production and the production cost of sinter. Finally, the consumption of energy in sintering production and the production cost of sinter have increased. The practice of some sintering plants has proved that the output can be increased by 6% when the air leakage rate is reduced by 10%, the power consumption can be reduced by 2 kW/h per ton of sinter, the coke powder can be reduced by 1 kg/t, and the finished product rate can be increased by 1.5%~2.0% [32–34]. Therefore, one of the most direct and effective ways to increase production, reduce consumption, and increase economic benefits in the sintering production process is to control the air leakage rate.

At present, the air leakage rate of various types of sintering equipment is generally about 50%, and the air leakage rate of some advanced enterprises is 40-45% during normal production. The difference in air leakage indicators of different enterprises is affected by various factors, but the main reason is that real-time online monitoring of air leakage cannot be performed, and then it is impossible to accurately determine the air leakage part of the sintering machine and carry out maintenance, which has become a common problem in the sintering industry. At present, the measurement of the air leakage rate of the sintering equipment is a general manual operation, which has a long measurement period and consumes more manpower and material resources, and the measurement results are greatly affected by production operation and working conditions [35]. If online monitoring can be realized, it will be of great help in the analysis of production status, operation, scheduling decision-making, and equipment maintenance. Both the oxygen content method and the colorimetric method can realize online detection and have been used in some factories [36]. The oxygen content method involves analyzing the air leakage rate of the sintering equipment system by detecting the oxygen content of the flue gas in the sintering flue. The oxygen content is detected by a zirconia analyzer, which is installed between the electrostatic precipitator and the bellows [37]. The principle of the calorimetric method is that the heat reserve change of exhaust gas leaving the system plus the heat loss of the system is equal to the heat of exhaust gas entering the system. To establish a heat balance formula, measure the temperature through thermocouples and calculate the air leakage rate according to the formula. Using deep learning to calculate the air leakage rate only requires a few easy-to-measure data points such as ignition temperature, airflow, and discharge temperature to calculate a more accurate air leakage rate [38]. The biggest advantage of neural networks is that they can continuously learn and improve to adapt to the prediction of air leakage rate under various conditions. A more rapid and accurate calculation of air leakage rate enables faster processing and maintenance, thereby improving production efficiency.

2. Proposed PSO-BP Combinatorial Model

In this section, we will firstly introduce the backpropagation (BP) based neural network model. Then, the particle swarm optimization (PSO) algorithm used in this study is described. Finally, the proposed PSO-BP combinatorial model is presented.

2.1. BP Neural Network Model. The BP neural network [39] is widely used in industrial control, and the basic idea of its model is to make real-time adjustments to the network weights by analyzing the network output error and gradient information, to further bring the network output closer and closer to the expected value. The BP neural network prediction model established in this paper uses the temperature and negative pressure data of 15 sintering processes to predict the air leakage rate, including ignition temperature, sintering machine speed, material layer thickness, and waste temperature. A complete neural network consists of three parts: an input layer, a hidden layer, and an output layer [40]. Figure 1 shows the structure of

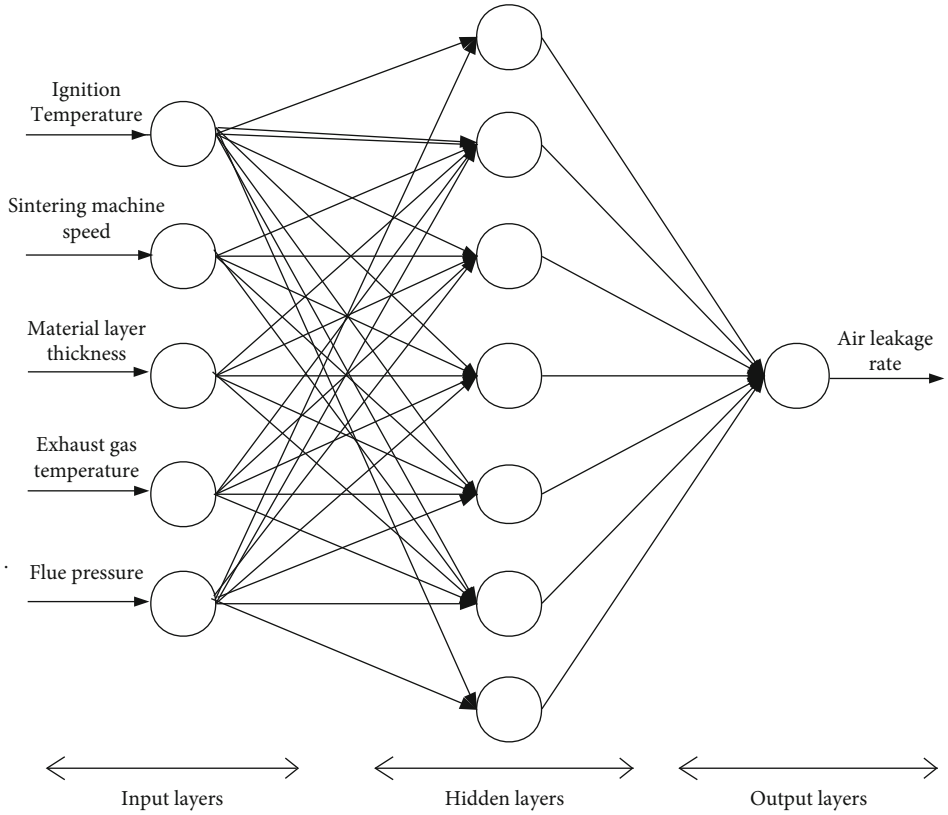

Figure 1: BP neural network structure.

the BP neural network used in this paper. $x_1 \sim x_{15}$ in the figure represents the input layer of the neural network; $w_1 \sim w_{15}$ represents the node weight of the input layer; $y_1 \sim y_7$ represents the node weight of the hidden layer; o is the output layer. In the neural network constructed by the algorithm used in this paper, the input layer includes 15 nodes whose actual meanings are ignition temperature, sintering machine speed, material layer thickness, waste temperature, etc. The prediction result of the air leakage rate of sintering equipment is the output layer, the number of hidden layer nodes selected according to the empirical formula $b = \sqrt{m+n} + a$, where m is the number of input nodes, n is the number of output nodes, a is a constant, and here we set it to 3. Therefore, the final number of hidden layer nodes b is 7.

As shown in the three-layer BP network above, the output H_j of the hidden layer is given in Equation (1):

$$H_j = g\left(\sum^{m} w_{ij}x_i + a_j\right). \tag{1}$$

The output of the output layer is shown in Equation (2):

$$O_k = \sum_{j=1}^{b} H_j w_{jk} + b_k. \tag{2}$$

In this paper, the error formula is taken as Equation (3):

$$E = \frac{1}{2}\sum_{k=1}^{n} (Y_k - O_k)^2. \tag{3}$$

The update formula of the weight is given in Equation (4):

$$\begin{cases} w_{ij} = w_{ij} + \eta H_j(1 - H_j)x_i \sum_{k-1}^{m} w_{jk}e_k \\ w_{jk} = w_{jk} + \eta H_j e_k \end{cases}. \tag{4}$$

BP neural network training is roughly divided into two processes: forward propagation and back propagation. After the forward propagation is completed, the error between the target value and the actual value is calculated, and then the internal weights and thresholds are continuously updated and adjusted through the back propagation of the error until the error is less than the initial set accuracy value. The training is completed, and the parameters can be used to predict air leakage rates [41]. The BP neural network is a kind of single-hidden-layer feedforward neural network. The weight and threshold of the network are iterated continuously by the gradient descent method, and finally, the data regression and classification are completed. However, in the initial state, the weights and thresholds of the network are arbitrarily set, and the system batching and control parameters

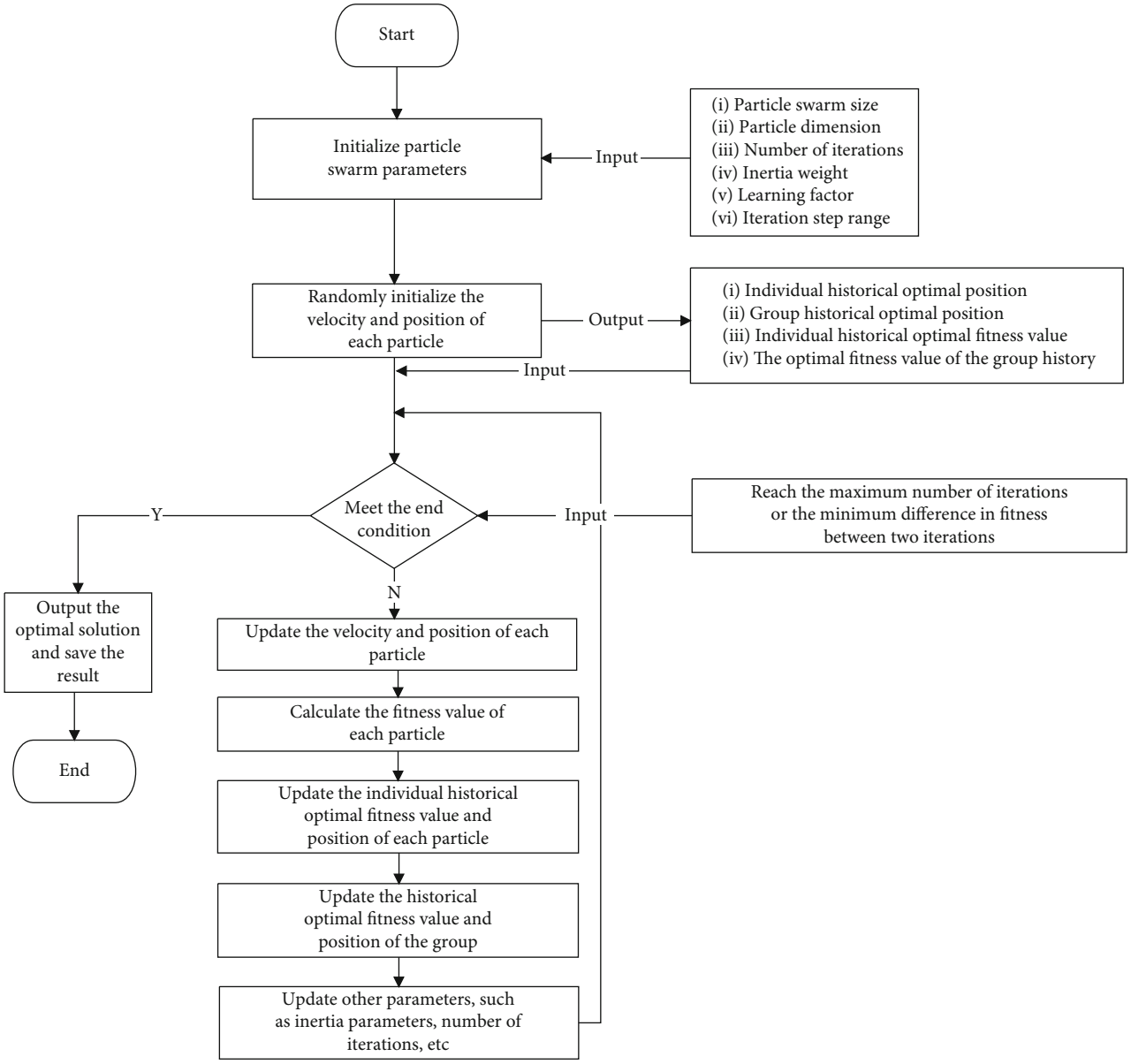

Figure 2: PSO model algorithm flow chart.

will be adjusted with the change of process requirements, which will lead to the difficulty of achieving optimal accuracy all the time. Therefore, this paper introduces the PSO algorithm to optimize the internal parameters to ensure that the prediction model is always in the optimal state.

Compared with other optimization algorithms, the PSO algorithm has the following advantages when optimizing neural networks: (1) for non-convex optimization problems such as neural network training, the stochastic optimization algorithm will have a stronger ability to explore the solution set space. (2) As a meta-heuristic algorithm, the implementation of PSO is relatively simple, and the calculation process is separated from the problem model. Many known modules of generic and meta-heuristic algorithms can be added to the PSO algorithm to improve its efficiency. (3) PSO is friendly to distributed computing and can effectively improve computing power. (4) Its speed updating mechanism, inertia, and other factors can be used to optimize the parameters of benchmarking neural networks for continuous optimization problems.

2.2. PSO Algorithm. The PSO algorithm [42] is a kind of swarm intelligence optimization algorithm that simulates individual birds through particles, the flow chart of which is presented in Figure 2. Particles communicate and cooperate with each other, constantly feeding back on their position and speed and updating them to find the optimal target solution.

Assuming that there is a $D-$ dimensional feasible space, the particle population number is N.

In the decision space, the current position of the i-th particle can be expressed as Equation (5):

$$x_i = (x_{i1}, x_{i2}, \cdots, x_{iD}), \tag{5}$$

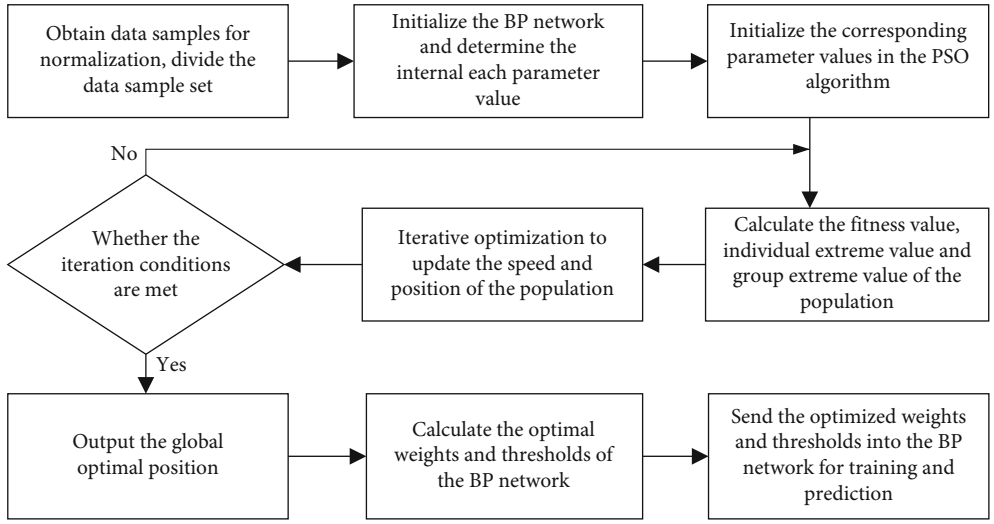

Figure 3: PSO-BP model algorithm flow chart.

where the particle x_i in this study represents one component (w_i) of the initial parameter w of the neural network. Each x_{ij} of a particle represents the w_i after j-th perturbation, and D is the predefined time for perturbation.

The current velocity of the i-th particle is Equation (6):

$$v_i = (v_{i1}, v_{i2}, \cdots, v_{iD}). \tag{6}$$

The best individual position of the i-th particle is Equation (7):

$$P\text{best} = (P_{i1}, P_{i2}, \cdots, P_{iD}). \tag{7}$$

The global optimal value in the whole search space is Equation (8):

$$g\text{best} = (g_1, g_2, \cdots g_D), \tag{8}$$

$$v_{\boxtimes D}^{k+1} = w_{\boxtimes D}^{k} + c_1 r_1 \left(P_{iD}^{k} - x_{iD}^{k}\right) + c_2 r_2 \left(P_{gD}^{k} - x_{gD}^{k}\right), \tag{9}$$

$$x_{\boxtimes D}^{k+1} = x_{\boxtimes D}^{k} + v_{\boxtimes D}^{k+1}. \tag{10}$$

At the same time, the velocity and position of the particles are updated according to the optimal value of each particle's feedback and the optimal value of the whole population [43]. The specific update formulas are shown in Equation (9) and Equation (10). In the formula: i represents the particle number; $v_{\boxtimes D}^{k+1}$ represents the speed of the particle at the next moment; w represents the inertia weight; $v_{\boxtimes D}^{k}$ represents the speed of the particle at the current moment; c_1, c_2 represent the learning factors; r_1, r_2 represent any numbers between [0, 1]; $p_{\boxtimes D}^{k}$ represents the current optimal position of the particle; p_{gD}^{k} represents the global optimal position of the particle; $x_{\boxtimes D}^{k}$ represents the current position of the particle; $x_{\boxtimes D}^{k+1}$ represents the next moment position of the particle [44].

2.3. Proposed PSO-BP Combinatorial Model. When a single BP neural network model is trained, the parameters such as initial weight and threshold are random, and then they are gradually modified in the iterative process. The initial parameters may have some negative effects on the training speed and training results, so we use a particle swarm optimization algorithm to optimize the initial parameters to improve the neural network [45].

Firstly, we use a few particles to simulate our initial parameters, assign the initial values, and then send them to the constructed network for an iteration. The initial loss of this training can be obtained, recorded, and set as the individual optimal value of the particle. Then, the position of the particle is updated according to the formula of velocity and position defined in Equations (9) and (10). After that, the loss is calculated again, so that the historical minimum loss, which represents the historical optimal position of the particle, will be updated. Multiple particles are searched at the same time, and the position is constantly changed to find the optimal position until the iterative conditions are met and the search stops. The optimal position found by particle swarm optimization is the best initial parameter value of the network, and then it is substituted into the BP neural network for training, and the final result is obtained. The flow chart of the PSO-BP [46] model establishment is shown in Figure 3.

3. Experimental Results and Analysis

A total of 1121 groups of air leakage rate data were collected in the experiment, among which the first 1010 groups of data were used to train the network, and the last 111 groups of data were used to test the training results. The exact values in the experiment are accurately measured by gas composition analysis [47], which is used to compare with our predicted data. The maximum iteration time of the BP neural network is 1000, the error accuracy is 0.05, the learning rate is 0.001, and the activation function is selected as logsig. At the same time, in the PSO algorithm,

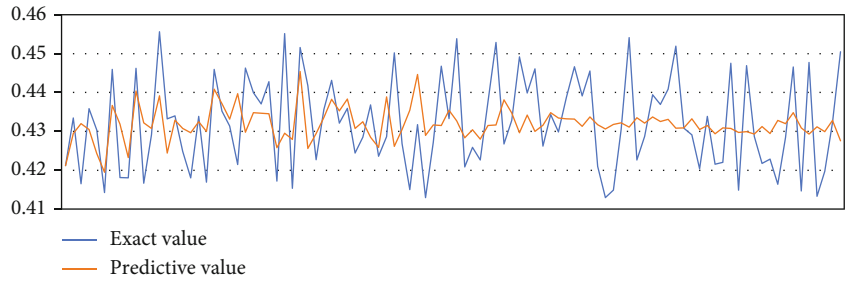

(a) Training set

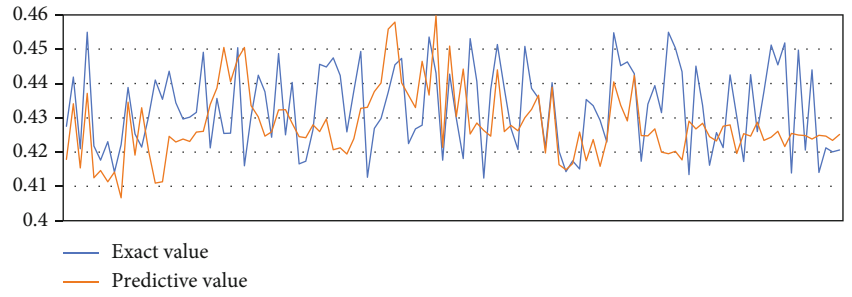

(b) Test set

Figure 4: A single BP network model.

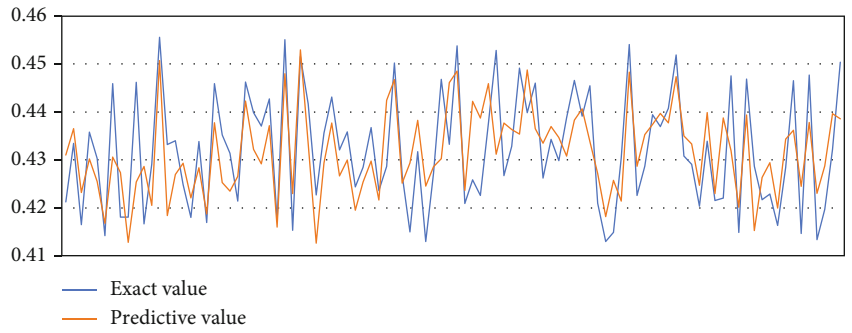

(a) Training set

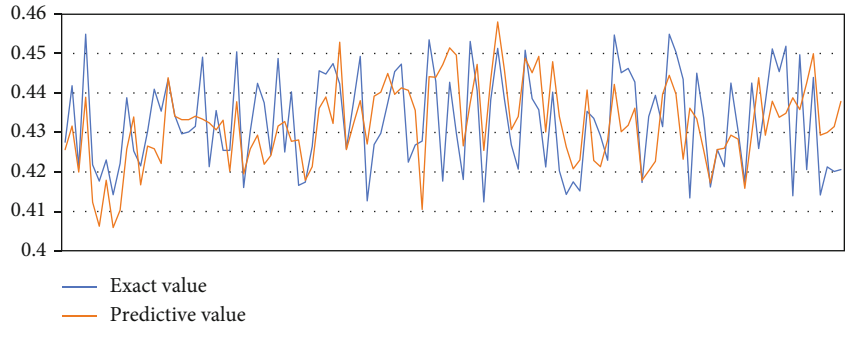

(b) Test set

Figure 5: PSO-BP model.

the parameter $c_1 = c_2 = 1.5$, the velocity boundary is [-1, 1], and the position boundary is [-5, 5]. The parameter D is set to 20, which indicates the maximum number of searches of the particle swarm algorithm. The definition of the regression coefficient is shown in Equation (11), and the value range is [0, 1]. The larger the value, the better the regression effect of the sample. In Equation (11): n represents the number of samples; x_i, y_i represents the sample data; $\bar{x}$, $\bar{y}$ represents the sample mean.

$$R = \frac{\sum_{i=1}^{n}(x_i - \bar{x})(y_i - \bar{y})}{\sqrt{\sum_{i=1}^{n}(x_i - \bar{x})^2 \times \sum_{i=1}^{n}(y_i - \bar{y})^2}}. \tag{11}$$

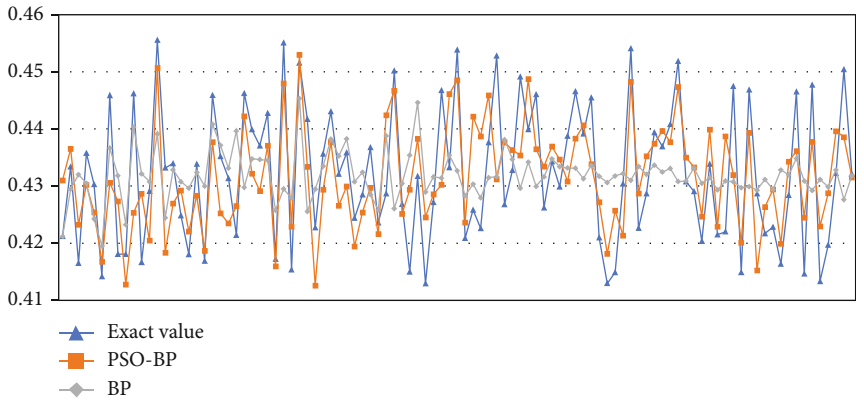

Figure 6: Comparison of the prediction model.

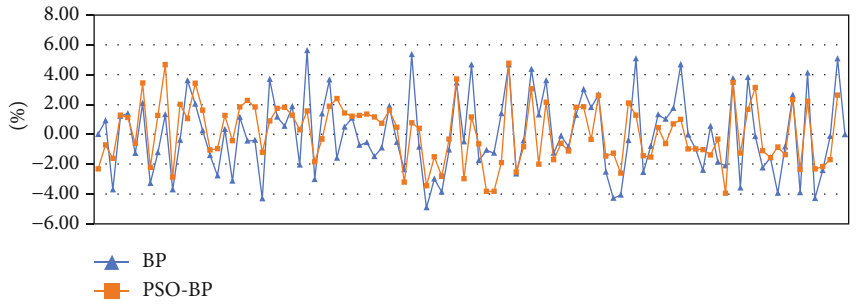

Figure 7: Comparison of prediction error.

Figure 4 shows the scatter plot of the predicted and actual values of air leakage rate trained by a single BP network model, and the regression coefficient at this time is R =0.764908. From the training results, each test sample cannot effectively fit the actual value completely, and the accuracy still needs to be improved. Therefore, the combined model after the BP network is optimized by introducing the PSO algorithm is being studied.

Figure 5 shows the scatter plot of the actual value and the predicted value after the BP neural network is optimized by the PSO algorithm. The regression coefficient is R =0.923661. It can be seen from the figure that the proposed model has good fitting ability.

To better understand the superiority of the proposed combined model prediction, the PSO-BP model is compared with the single BP neural network model, and the results are shown in Figures 6 and 7. According to Figures 6 and 7, it can be seen that the proposed BP neural network model optimized by the PSO algorithm has greatly improved the prediction accuracy. Because of the randomness of weights and thresholds in the BP network at the initial stage, the parameters are not optimal, so the optimal values of the particle population are searched for by the particle swarm optimization algorithm, and the optimal weights and thresholds in the network are calculated. The optimized parameters are then re-sent to the BP network for training and prediction, and the results are greatly improved. The latter parameters are sent back to the BP network for training and prediction, and the results have been greatly improved.

Table 1: Comparison of evaluation indexes of single BP and PSO-BP model.

Predictive model	RMSE	MAE	MAPE
BP	0.01131	0.00922	0.02128
PSO-BP	0.00864	0.00743	0.01718

To further verify the accuracy of the prediction, an error indicator can be introduced for further verification. The commonly used error indicators include root mean square error, average absolute error, and average absolute percentage error. Therefore, this paper uses these three evaluation indicators to evaluate the superiority of the model. The comparison of evaluation indicators is shown in Table 1. From the table, it can be clearly seen that the error index after the combination of the two models has been greatly improved based on the original single model, which provides an effective basis for verifying the accuracy of the combined model proposed in this paper.

4. Conclusions

This paper aims to solve the problem of air leakage in the sintering process of the sintering furnace. We propose a neural network model based on PSO-BP and conduct a series of comparative experiments with the ordinary BP neural network model. The experimental results indicate that we have found promising weights and thresholds for the proposed neural network model through the designed optimization

method, where the regression coefficient of the training results is significantly improved. In addition, the indicator results referring to RMSE, MAE, and MAPE have demonstrated that the accuracy of the proposed PSO-BP neural network model has increased by 23.607%, 19.414%, and 19.267%, respectively, in comparison with the traditional BP neural network model. At present, this algorithm still has some shortcomings. The training of the BP neural network is often stagnant in the flat area of the error gradient surface, and the convergence speed is slow and may even fail to converge. We plan to improve it in the future by adapting the learning rate, increasing the learning rate where the error gradient is flat, and decreasing it otherwise, so that the algorithm can converge better.

Data Availability

The code of the proposed algorithm and corresponding experimental data are provided. Interested readers please visit: https://github.com/Darrenquan/Prediction-of-air-leakage-rate.

Conflicts of Interest

The authors declare that there is no conflict of interest regarding the publication of this paper.

Acknowledgments

This work was supported in part by the Fundamental Research Funds for the Central Universities No. N2117005, the Joint Funds of the Natural Science Foundation of Liaoning Province under grant No. 2021-KF-11-01, the Fundamental Research Funds for the Central Universities, the National Natural Science Foundation of China under grant No. 62103150, and the project funded by China Postdoctoral Science Foundation under grant No. 2021M691012.

References

[1] Z. Yuan, B. Wang, K. Liang, Q. Liu, and L. Zhang, "Application of deep belief network in the prediction of secondary chemical components of sinter," in *2018 13th IEEE Conference on Industrial Electronics and Applications (ICIEA)*, pp. 2746–2751, May 2018.

[2] S. G. Savel'ev, "Dependence of sinter strength on the sintering rate," *Steel Transl.*, vol. 41, no. 10, pp. 826–829, 2011.

[3] X. Xue, J. Chen, and X. Yao, "Efficient user involvement in semiautomatic ontology matching," *IEEE Transactions on Emerging Topics in Computational Intelligence*, vol. 5, no. 2, pp. 214–224, 2021.

[4] Y. Z. Wang, J. L. Zhang, Z. J. Liu, and C. B. Du, "Recent advances and research Ssatus in energy conservation of iron ore sintering in China," *JOM*, vol. 69, pp. 2404–2411, 2017.

[5] L. Ma, S. Cheng, and Y. Shi, "Enhancing learning efficiency of brain storm optimization via orthogonal learning design," *IEEE Transactions on Systems, Man, and Cybernetics: Systems*, vol. 51, no. 11, pp. 6723–6742, 2021.

[6] D. H. Liu, H. Liu, J. L. Zhang et al., "Basic characteristics of Australian iron ore concentrate and its effects on sinter properties during the high-limonite sintering process," *International Journal of Minerals, Metallurgy, and Materials*, vol. 24, pp. 991–998, 2017.

[7] L. Ma, M. Huang, S. Yang, R. Wang, and X. Wang, "An adaptive localized decision variable analysis approach to large-scale multiobjective and many-objective optimization," *IEEE Transactions on Cybernetics*, 2021.

[8] C. Yang, T. Wei, X. Dong, Y. Li, S. Qu, and X. Li, "Sinter-hardening with concurrent improved plasticity in iron alloys induced by spark plasma sintering," *Journal of Materials Research*, vol. 29, pp. 981–988, 2014.

[9] L. Ma, X. Wang, X. Wang, L. Wang, Y. Shi, and M. Huang, "TCDA: truthful combinatorial double auctions for mobile edge computing in industrial internet of things," *IEEE Transactions on Mobile Computing*, 2021.

[10] Y. X. Xue, D. Q. Zhu, J. Pan et al., "Significant influence of self-possessed moisture of limonitic nickel laterite on sintering performance and its action mechanism," *Journal of Iron and Steel Research International*, pp. 1–13, 2022.

[11] L. Lu and J. Manuel, "Sintering characteristics of iron ore blends containing high proportions of Goethitic ores," *JOM*, vol. 73, no. 1, pp. 306–315, 2021.

[12] L. Ma, N. Li, Y. Guo et al., "Learning to optimize: reference vector reinforcement learning adaption to constrained many-objective optimization of industrial copper burdening system," *IEEE Transactions on Cybernetics*, 2021.

[13] A. Szewczyk-Nykiel and R. Bogucki, "Sinter-bonding of AISI 316L and 17-4 PH stainless steels," *J. of Materi Eng and Perform*, vol. 27, no. 10, pp. 5271–5279, 2018.

[14] L. Ma, X. Wang, M. Huang, Z. Lin, L. Tian, and H. Chen, "Two-level master-slave RFID networks planning via hybrid multi-objective artificial bee colony optimizer," *IEEE Transactions on Systems, Man, and Cybernetics: Systems*, vol. 49, no. 5, pp. 861–880, 2019.

[15] L. S. Pan, X. L. Wei, Y. Peng, X. B. Shi, and H. L. Liu, "Experimental study on convection heat transfer and air drag in sinter layer," *Journal of Central South University*, vol. 22, pp. 2841–2848, 2015.

[16] J. S. Feng, H. Dong, J. Y. Gao, J. Y. Liu, and K. Liang, "Theoretical and experimental investigation on vertical tank technology for sinter waste heat recovery," *Journal of Central South University*, vol. 24, pp. 2281–2287, 2017.

[17] X. Xue and J. Zhang, "Matching large-scale biomedical ontologies with central concept based partitioning algorithm and adaptive compact evolutionary algorithm," *Applied Soft Computing*, vol. 106, article 107343, 2021.

[18] Y. Frolov, A. Nokesh, and L. Polotskii, "Study of flue-gas recirculation sintering," *Study of Flue-Gas Recirculation Sintering. Metallurgist*, vol. 61, no. 7-8, pp. 629–637, 2017.

[19] C. Kuo, S. Qiu, and X. Yang, "A low-cost and highly efficient method of reducing coolant leakage for direct metal printed injection mold with cooling channels using optimum heat treatment process procedures," *International Journal of Advanced Manufacturing Technology*, vol. 115, no. 7-8, pp. 2553–2570, 2021.

[20] W. Zhang, S. Wu, and Z. Hu, "Analysis of operational parameters affecting denitrification rate of sintering flue gas in cross-flow activated coke purification facility," *Journal of Iron and Steel Research, International*, vol. 27, no. 8, pp. 887–897, 2020.

[21] C. Nahm, "Sintering effect on varistor properties and degradation behavior of ZVMB varistor ceramics," *Journal of*

Materials Science: Materials in Electronics, vol. 28, no. 22, pp. 17063–17069, 2017.

[22] J. Park and C. Nahm, "Sintering effect on electrical properties and aging behavior of quaternary ZnO–V2O5–Mn3O4–Nb2O5 ceramics," *Journal of Materials Science: Materials in Electronics*, vol. 26, no. 1, pp. 168–175, 2015.

[23] F. Y. Tian, L. F. Huang, L. W. Fan et al., "Pressure drop in a packed bed with sintered ore particles as applied to sinter coolers with a novel vertically arranged design for waste heat recovery," *Journal of Zhejiang University-SCIENCE A*, vol. 17, pp. 89–100, 2016.

[24] S. Sharma, H. Sharma, S. Kumar, S. Thakur, R. K. Kotnala, and N. S. Negi, "Analysis of sintering temperature effects on structural, dielectric, ferroelectric, and piezoelectric properties of BaZr0.2Ti0.8O3 ceramics prepared by sol–gel method," *Journal of Materials Science: Materials in Electronics*, vol. 31, pp. 19168–19179, 2020.

[25] G. H. Chen, J. L. Li, X. Chen, X. L. Kang, and C. L. Yuan, "Sintering temperature dependence of varistor properties and impedance spectroscopy behavior in ZnO based varistor ceramics," *Journal of Materials Science: Materials in Electronics*, vol. 26, pp. 2389–2396, 2015.

[26] C. Nahm, "Sintering temperature dependence on microstructure and non-ohmic properties of ZVMND ceramic semiconductors," *Journal of Materials Science: Materials in Electronics*, vol. 27, no. 9, pp. 9520–9525, 2016.

[27] J. G. Fisher, M. G. Kim, D. Kim et al., "Reactive sintering of (K0.5Bi0.5) TiO3-BiFeO3 lead-free piezoelectric ceramics," *Journal of the Korean Physical Society*, vol. 66, pp. 1426–1438, 2015.

[28] X. Xue and C. Jiang, "Matching sensor ontologies with multi-context similarity measure and parallel compact differential evolution algorithm," *IEEE Sensors Journal*, vol. 21, no. 21, pp. 24570–24578, 2021.

[29] Q. He, X. Wang, Z. Lei, M. Huang, Y. Cai, and L. Ma, "TIFIM: a two-stage iterative framework for influence maximization in social networks," *Applied Mathematics and Computation*, vol. 354, pp. 338–352, 2019.

[30] X. Y. Wu, J. R. Liu, Y. Chen, and M. H. Wang, "Effect of B2O3 concentration and sintering temperature on microstructure and electrical properties in the ZnO-Bi2O3-based varistors," *Journal of Electronic Materials*, vol. 48, pp. 7704–7709, 2019.

[31] C. Nahm, "Microstructure and electrical properties of ZnO–Pr6O11–Bi2O3-based varistor ceramics with sintering changes," *Journal of Materials Science: Materials in Electronics*, vol. 26, no. 11, pp. 8380–8385, 2015.

[32] Z. Q. Tan, U. Engström, K. Li, and Y. Liu, "Effect of furnace atmosphere on sintering process of chromium-containing steel via powder metallurgy," *Journal of Iron and Steel Research International*, vol. 28, pp. 889–900, 2021.

[33] Z. Wang, Y. Huan, H. Wang et al., "The optimal sintering atmosphere and defect structure of CuO-doped NKN-based ceramic with p/n-type conduction mechanism," *Journal of Materials Science: Materials in Electronics*, vol. 32, pp. 1928–1940, 2021.

[34] L. Zhao, W. Sun, X. Li et al., "Assessment of particulate emissions from a sinter plant in steelmaking works in China," *Environmental Monitoring and Assessment*, vol. 189, no. 8, pp. 1–16, 2017.

[35] Y. Z. Wang, J. L. Zhang, Z. J. Liu, Y. P. Zhang, D. H. Liu, and Y. R. Liu, "Characteristics of combustion zone and evolution of mineral phases along bed height in ore sintering," *International Journal of Minerals, Metallurgy, and Materials*, vol. 24, pp. 1087–1095, 2017.

[36] W. D. Tang, S. T. Yang, L. H. Zhang, Z. Huang, H. Yang, and X. X. Xue, "Effects of basicity and temperature on mineralogy and reduction behaviors of high-chromium vanadium-titanium magnetite sinters," *Journal of Central South University*, vol. 26, pp. 132–145, 2019.

[37] J. Li, D. Bhattacharjee, X. Hu, D. Zhang, S. Sridhar, and Z. Li, "Effects of slag composition on H2 generation and magnetic precipitation from molten steelmaking slag–steam reaction," *Metallurgical and Materials Transactions B*, vol. 50, pp. 1023–1034, 2019.

[38] M. Sharma and N. Dogan, "Dissolution behavior of aluminum titanate inclusions in steelmaking slags," *Metallurgical and Materials Transactions B: Process Metallurgy and Materials Processing Science*, vol. 51, no. 2, pp. 570–580, 2020.

[39] X. Xue, J. Lu, and J. Chen, "Using NSGA-III for optimising biomedical ontology alignment," *CAAI Transactions on Intelligence Technology*, vol. 4, no. 3, pp. 135–141, 2019.

[40] K. Zhang, F. Yuan, J. Guo, and G. Wang, "A novel neural network approach to transformer fault diagnosis based on momentum-embedded BP neural network optimized by genetic algorithm and fuzzy c-means," *Arabian Journal for Science and Engineering*, vol. 41, pp. 3451–3461, 2016.

[41] S. Xu, "Retraction note to: BP neural network–based detection of soil and water structure in mountainous areas and the mechanism of wearing fatigue in running sports," *Arabian Journal of Geosciences*, vol. 14, no. 22, p. 2403, 2021.

[42] G. Singh and K. Deep, "Effectiveness of new multiple-PSO based membrane optimization algorithms on CEC 2014 benchmarks and iris classification," *Natural Computing*, vol. 16, no. 3, pp. 473–496, 2017.

[43] D. K. Choubey, P. Kumar, S. Tripathi, and S. Kumar, "Performance evaluation of classification methods with PCA and PSO for diabetes," *Network Modeling Analysis in Health Informatics and Bioinformatics*, vol. 9, pp. 1–30, 2020.

[44] B. Yang and L. Cheng, "Study of a new global optimization algorithm based on the standard PSO," *Journal of Optimization Theory and Applications*, vol. 158, no. 3, pp. 935–944, 2013.

[45] Y. Sun and Q. Zhang, "Optimization design and reality of the virtual cutting process for the boring bar based on PSO-BP neural networks," *Neural Computing and Applications*, vol. 29, no. 5, pp. 1357–1367, 2018.

[46] T. Bai, H. Meng, and J. Yao, "A forecasting method of forest pests based on the rough set and PSO-BP neural network," *Neural Computing and Applications*, vol. 25, no. 7-8, pp. 1699–1707, 2014.

[47] Y. Bernaldo de Quirós, O. González-Díaz, A. Møllerløkken et al., "Differentiation at autopsy between in vivo gas embolism and putrefaction using gas composition analysis," *International Journal Of Legal Medicine*, vol. 127, pp. 437–445, 2013.